Nontrivial Phase Behaviour in the Infinite-Range Quantum Mattis Model

P. Sollich, Hidetoshi Nishimori[1], A. C. C. Coolen
and A. J. van der Sijs[2]*

Department of Mathematics, King's College London, Strand, London WC2R 2LS, United Kingdom
[1]*Department of Physics, Tokyo Institute of Technology, Oh-okayama, Meguro-ku, Tokyo 152-8551*
[2]*Department of Physics, University of Oxford, 1 Keble Road, Oxford OX1 3NP, United Kingdom*

We have solved the quantum version of the Mattis model with infinite-range interactions. A variational approach gives the exact solution for the infinite-range system, in spite of the non-commutative nature of the quantum spin components; this implies that quantum effects are not predominant in determining the macroscopic properties of the system. Nevertheless, the model has a surprisingly rich phase behaviour, exhibiting phase diagrams with tricritical, three-phase and critical end points.

KEYWORDS: Quantum spin, Mattis model, randomness, infinite-range model, exact solution, variational method

§1. Introduction

Quantum spin systems with randomness are of active current interest because the interplay of randomness and quantum fluctuations often leads to nontrivial behaviour.[1,2] However, full exact analysis of such systems is very difficult, partly due to the randomness and partly due to non-commutativity of quantum spin operators. We therefore solve in the present paper a quantum version of the Mattis model with infinite-range interactions to investigate the effects of coexistence of randomness and quantum fluctuations.

The Mattis model was originally proposed as a simple spin glass model exhibiting only randomness, but no frustration.[3] It consists of Ising spins interacting via unfrustrated random exchange interactions. The randomness can be gauged away, giving a simple ferromagnetic Ising model. The model is nevertheless nontrivial under an external field, in which case the problem reduces to that of the Ising ferromagnet with random local fields. In this paper we study the *quantum* version of the Mattis model in an external field. This is a more complex problem because, even in the absence of external fields, one cannot gauge away the randomness in the exchange interactions without violating the commutation relations of the quantum spin operators.

There have been several investigations of the quantum Mattis model including the dispersion relation[4] and the symmetry of the ground-state.[5] These studies show that the non-commutativity of spin operators does not necessarily play an important role in the determination of the qualitative behaviour of the system. However, there has to date been no explicit solution for the equilibrium behaviour of the infinite-range model, even without an external field. The exact solution given in the present paper fills this gap; it also shows explicitly that, as was to be expected from the earlier studies cited above,[4,5] quantum fluctuations do not affect the structure of the phase diagram in an essential way. The physical reason for this fact is that the effective field acting on a spin is the sum of very many other spins when the range of interactions is infinite; but the sum of many quantum spin operators behaves like a classical vector. Hence, as we show, the problem reduces effectively to that of a single-site quantum spin in a classical external field.

In spite of this fact, the system exhibits very rich phase behaviour. There are essentially three ordered phases, two with collinear spin orientations (parallel or antiparallel to the external field), and one with non-collinear spins. These phases are separated by first or second order transition lines which terminate or meet at critical, tricritical, three-phase or critical end points. All these types of phase behaviour can be explicitly and exactly derived by relatively simple but nevertheless nontrivial manipulations.

The paper is organized as follows. The model is defined and its variational free energy is derived in §2. Extremization of the variational free energy gives the exact solution of the infinite-range model, even for quantum spins. (In an appendix, we also confirm the variational result by a direct explicit calculation.) The three special cases of the Ising, Heisenberg and *XY* models, which already exhibit the three types of ordered phases mentioned above, are treated in §3. In §4, then, the model is analysed for general values of the anisotropy parameter in the exchange interaction. While no additional ordered phases appear, the resulting phase diagrams now exhibit new and nontrivial features such as tricritical, three-phase and critical end points. The final section is devoted to conclusions.

§2. Model and Free Energy

The system we consider consists of N spin-1/2 quan-

---

* Present address: ASM Litography, PO Box 324, NL-5500 AH Veldhoven, The Netherlands.

tum spins S_i. We use the rescaled spins $\sigma_i = (2/\hbar)S_i$, whose components have eigenvalues $\sigma_i^\alpha = \pm 1$ ($\alpha = x, y, z$), to describe the state of the system; this makes correspondences with classical Ising models easier to see. The Hamiltonian is defined as

$$H = -\frac{1}{N}\sum_{i<j}\xi_i\xi_j\sigma_i \cdot \mathrm{J}\,\sigma_j - \sum_i \mathrm{B} \cdot \sigma_i. \tag{2.1}$$

Here the sum runs over all pairs of sites, J is a general 3×3 coupling matrix, B is an external field, and the $\xi_i = \pm 1$ are quenched random variables. If only J_{zz} and B_z are nonzero, then only the z-components of the spins, σ_i^z, appear in H. Because the σ_i^z all commute with each other, the quantum nature of the problem is then irrelevant, and one recovers the classical Mattis model[3] which is formulated in terms of Ising spins.

It should be noted that the infinite-range model does not have a lattice structure, and consequently the concept of randomness in ξ_i does not have its direct significance. In fact, the present model is identical to a two-sublattice infinite-range model with all bonds within a sublattice being ferromagnetic and all bonds between different sublattices antiferromagnetic. Randomness does not play an explicit role here. Nevertheless, such an infinite-range model can serve as a mean-field approximation to the Mattis model in finite dimensions with real randomness. This is clear from the case of the ferromagnetic Ising model in a random field, which is equivalent to the classical Mattis model in a uniform field.[6] We therefore retain the terminology of randomness and disorder in the following.

To solve the model (2.1), it is tempting to try to gauge away the quenched disorder by the transformation $\sigma_i \to \xi_i\sigma_i$. But this is impossible, because the gauged spins would no longer obey the required commutation relations

$$[\sigma_i^\alpha, \sigma_i^\beta] = 2i\sum_\gamma \epsilon_{\alpha\beta\gamma}\sigma_i^\gamma, \tag{2.2}$$

with $\epsilon_{\alpha\beta\gamma}$ the fully antisymmetric unit tensor. Instead, we solve the model using a variational mean field theory which treats the spins as uncorrelated with each other. Because we are dealing with a model with infinite range interactions, this approximation becomes exact in the thermodynamic limit $N \to \infty$; an explicit self-consistency argument for this fact is given in Appendix A. A direct solution of a special case given in Appendix B also confirms the variational result. We note that Duffield $et\ al.$[7] have given a unified treatment of a large class of long-range quantum spin systems with site disorder (including the one we consider) and derived an expression for the free energy by mathematically rigorous techniques. The fact that their result coincides with our variational calculation is probably the most direct confirmation of its exactness.

In the mean field approach, we start from a trial Hamiltonian

$$H_0 = -\sum_i \mathrm{h}_i \cdot \sigma_i$$

with the associated variational free energy

$$\tilde{F} = F_0 + \langle H - H_0\rangle_0\,.$$

Here $\langle\ldots\rangle_0$ denotes an average over the Boltzmann distribution defined by H_0, and F_0 is the corresponding free energy. The fact that mean field theory is exact then means that the minimum of $\tilde{F}$ with respect to the h_i is not just an upper bound on the true free energy F, but in fact equal to it in the thermodynamic limit. One easily evaluates $\tilde{F}$ as

$$\tilde{F} = -T\sum_i \ln 2\cosh\beta|\mathrm{h}_i|$$
$$-\frac{1}{N}\sum_{i<j}\xi_i\xi_j\mathrm{m}_i \cdot \mathrm{J}\,\mathrm{m}_j - \sum_i (\mathrm{B} - \mathrm{h}_i)\cdot \mathrm{m}_i,$$

where $\beta = 1/T$ as usual. The magnetizations are given by

$$\mathrm{m}_i = \langle\sigma_i\rangle_0 = \mathrm{t}(\beta\mathrm{h}_i),$$

in terms of the "vector hyperbolic tangent"

$$\mathrm{t}(\mathrm{v}) = \frac{\mathrm{v}}{|\mathrm{v}|}\tanh(|\mathrm{v}|).$$

Minimizing $\tilde{F}$ with respect to the h_i gives the conditions

$$\chi_i\left[\mathrm{h}_i - \mathrm{B} - \xi_i\frac{1}{N}\sum_{j\neq i}\xi_j\mathrm{J}\,\mathrm{m}_j\right] = 0 \tag{2.3}$$

where the χ_i are the local susceptibility tensors

$$\chi_i = \frac{\partial\mathrm{m}_i}{\partial\mathrm{h}_i}$$

the sublattice magnetizations alone, with the result

$$
\begin{aligned}
&\tilde{f}(\mathrm{m}_+, \mathrm{m}_-) \\
&= -Tn_+ s(|\mathrm{m}_+|) - Tn_- s(|\mathrm{m}_-|) \\
&\quad - \frac{1}{2}(n_+\mathrm{m}_+ - n_-\mathrm{m}_-) \cdot \mathrm{J}(n_+\mathrm{m}_+ - n_-\mathrm{m}_-) \\
&\quad - \mathrm{B} \cdot (n_+\mathrm{m}_+ + n_-\mathrm{m}_-),
\end{aligned}
\tag{2.6}
$$

where the entropic contribution is expressed as usual in terms of the entropy of a binary distribution,

$$
s(m) = -\frac{1+m}{2}\ln\frac{1+m}{2} - \frac{1-m}{2}\ln\frac{1-m}{2}.
\tag{2.7}
$$

The true free energy per spin is obtained as the minimum of the variational free energy, hence the final result

$$
f = \min_{\mathrm{m}_+, \mathrm{m}_-} \tilde{f}(\mathrm{m}_+, \mathrm{m}_-).
\tag{2.8}
$$

In the following, because the variational free energy is exact for $N \to \infty$, we drop the tilde on $\tilde{f}$. The requirement that $f(\mathrm{m}_+, \mathrm{m}_-)$ must be stationary with respect to m_+ and m_- gives two self-consistency equations which can be written in the compact (and intuitively appealing) form

$$
\mathrm{m}_+ = \mathrm{t}[(n_+\mathrm{J}\mathrm{m}_+ - n_-\mathrm{J}\mathrm{m}_- + \mathrm{B})/T]
\tag{2.9}
$$

$$
\mathrm{m}_- = \mathrm{t}[(-n_+\mathrm{J}\mathrm{m}_+ + n_-\mathrm{J}\mathrm{m}_- + \mathrm{B})/T].
\tag{2.10}
$$

We emphasize that the energetic terms in the free energy (2.6) are exactly of the form that one would expect if the sublattice spins

$$
\frac{3}{4}_\pm = \frac{1}{Nn_\pm}\sum_{i\in I_\pm} \frac{3}{4}_i,
$$

were classical vectors rather than quantum operators. Working out commutation relations such as

$$
\begin{aligned}
[\sigma_+^\alpha, \sigma_+^\beta] &= \frac{1}{N^2 n_+^2}\sum_{i,j\in I_+}[\sigma_i^\alpha, \sigma_i^\beta] \\
&= \frac{1}{N^2 n_+^2}\sum_{i\in I_+} 2i\sum_\gamma \epsilon_{\alpha\beta\gamma}\sigma_i^\gamma \\
&= \frac{2i}{Nn_+}\sum_\gamma \epsilon_{\alpha\beta\gamma}\sigma_+^\gamma
\end{aligned}
$$

indeed shows that in the thermodynamic limit $N \to \infty$ the vectors $\frac{3}{4}_\pm$ become classical, with all components commuting with each other. Note that even though the $\mathrm{m}_\pm$ are classical, the quantum (spin) nature of the problem is still reflected in the functional form (2.7) of the entropic contribution to the free energy (2.6).

Having derived the free energy of our model for general J and B, we specialize from now on to the case

$$
\mathrm{J} = \mathrm{diag}(1,1,\Delta), \quad \mathrm{B} = (0,0,B).
\tag{2.11}
$$

The parameter Δ here interpolates between three important limits: For $\Delta = 0$ and 1, respectively, we have the XY and Heisenberg versions of the model, while for $\Delta \to \infty$ the classical (Ising) Mattis model is recovered. We will analyse these three cases separately first before studying the richer behaviour obtained for intermediate values of Δ. Because all phase diagrams are symmetric

under $B \to -B$, we generally restrict ourselves to $B \geq 0$.

Finally, before proceeding, we note that with the choice (2.11), the model has a trivial rotational symmetry in the xy-plane. We break this symmetry by requiring that $m_+^y = 0$ and $m_+^x \geq 0$. Minimization of (2.6) with respect to rotations of m_- implies that the components of m_+ and m_- in the xy-plane are antiparallel to each other, thus also $m_-^y = 0$, and $m_-^x \leq 0$. So the minimization in (2.8) only has to be carried out over the four magnetization components m_+^z, m_-^z, m_+^x, m_-^x, with the latter being respectively non-negative and non-positive. We also assume throughout that the positive sublattice I_+ contains more spins than the negative one, i.e., $n_+ > n_-$, and take $n_- > 0$ in order to exclude the trivial case of an anisotropic quantum ferromagnet without disorder. Instead of n_+ and n_-, we will sometimes use the parameter ϵ, defined by $n_\pm = (1 \pm \epsilon)/2$; $\epsilon \to 1$ then corresponds to the disorder-free limit, and our assumptions on n_+ and n_- translate into $0 < \epsilon < 1$.

§3. Ising, Heisenberg and XY Models

3.1 Ising limit ($\Delta \to \infty$)

In the limit $\Delta \to \infty$, the free energy (2.6) is minimized when the sublattice magnetizations point along the z-axis. We thus only have two nonzero order parameters m_+^z and m_-^z to consider, and effectively recover the Mattis model with classical Ising spins. Using $s(m) = s(-m)$, the free energy simplifies to

$$
\begin{aligned}
f/\Delta &= -\tilde{T}n_+ s(m_+^z) - \tilde{T}n_- s(m_-^z) \\
&\quad - \frac{1}{2}(n_+ m_+^z - n_- m_-^z)^2 - \tilde{B}(n_+ m_+^z + n_- m_-^z),
\end{aligned}
\tag{3.1}
$$

and the stationarity conditions (2.9) and (2.10) become

$$
m_+^z = \tanh[(n_+ m_+^z - n_- m_-^z + \tilde{B})/\tilde{T}]
\tag{3.2}
$$

$$
m_-^z = \tanh[(-n_+ m_+^z + n_- m_-^z + \tilde{B})/\tilde{T}].
\tag{3.3}
$$

Here we have introduced the rescaled temperature $\tilde{T} = T/\Delta$ and field $\tilde{B} = T/\Delta$ which are the relevant control parameters for $\Delta \to \infty$.

Considering first the zero temperature limit $\tilde{T} \to 0$, the only possible solutions of (3.2) and (3.3) are $m_\pm^z = \pm 1$, so we only need to compare the four resulting values of f. For large $\tilde{B}$, one finds in this way that $m_+^z = m_-^z = 1$. We call this phase A_+, to indicate that both sublattice magnetizations m_+ and m_- are *aligned* along the direction of the field B, with both pointing in the same direction. At $\tilde{B} = n_+$, there is a first order transition to $m_+^z = 1$, $m_-^z = -1$; we denote this new phase A_- because the sublattice magnetizations, while still aligned with the field, now point in opposite directions. Finally, at $\tilde{B} = 0$ we have the conventional first order transition where both magnetizations change sign, and then the mirror image of the A_+–A_- transition occurring at $\tilde{B} = -n_+$. As pointed out earlier, all phase diagrams of our model have this symmetry under $B \to -B$, so we will not mention results for $B < 0$ in the following.

In the $\tilde{T}$-$\tilde{B}$ phase diagram, the first order transitions found above for $\tilde{T} = 0$ mark the beginnings of two first order transition lines, both ending in critical points. The
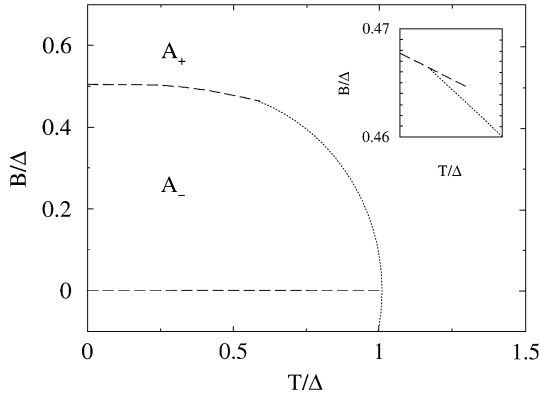
Fig. 1. Phase diagram for the Ising limit $\Delta \to \infty$, for $\epsilon = 0.01$. The dashed lines indicate first order transitions, and end in critical points. The transition at $B/\Delta = 0$ and $T/\Delta < 1$ is a conventional one, where all magnetizations change sign; at the other transition ($B/\Delta \neq 0$), the relative orientation of the sublattice magnetizations changes from antiparallel (A_-) to parallel (A_+). The dotted line indicates the points where the A_- and A_+ phases transform smoothly into each other as m_-^z passes through zero. As the inset shows, the A_-–A_+ critical point is not on this line; it has $m_-^z > 0$.

general procedure by which we find such points is outlined in Appendix D; after a little algebra, the two relevant conditions (D·2) and (D·5) become

$$\tilde{T} = n_+[1 - (m_+^z)^2] + n_-[1 - (m_-^z)^2]$$
$$0 = n_+ m_+^z[1 - (m_+^z)^2] - n_- m_-^z[1 - (m_-^z)^2]. \quad (3.4)$$

These need to be solved along with (3.2) and (3.3). The critical point that marks the end of the first order transition line at $\tilde{B} = 0$ has $m_+^z = m_-^z = 0$ and is thus located at $\tilde{T} = n_+ + n_- = 1$, $\tilde{B} = 0$. The critical point terminating the A_+–A_- transition line, on the other hand, has to be found numerically, along with the location of that line itself. The resulting phase diagram is shown in Fig. 1 for $\epsilon = 0.01$.

Note that because of the critical point terminating the line of first order transitions between A_+ and A_-, these two phases can be smoothly transformed into one another by moving along a continuous path in the $\tilde{T}$-$\tilde{B}$ phase diagram. Along this path, the value of m_-^z changes sign by passing through zero; the points where this happens obey $\tilde{B} = n_+ \tanh(2\tilde{B}/\tilde{T})$, as is easily derived from (3.2) and (3.3). As in the case of the liquid-gas transition, this makes the thermodynamic distinction between the two phases somewhat arbitrary. Unlike the traditional case, however, the critical point is not due to a symmetry under sign reversal of the magnetization; the critical value of m_-^z is therefore nonzero (and, by (3.4), positive). This implies that just below the critical temperature, the A_+–A_- transition is actually between two phases with $m_-^z > 0$, rather than two phases with opposite signs of m_-^z.

The case of $\epsilon = 0$ in the Ising limit is worth an attention although we generally assume $\epsilon > 0$. When $\epsilon = 0$, the system is equivalent to the random-field Ising model with symmetric distribution of randomness. This problem has already been solved by the mean-field approx-

imation.[8] The phase diagram is similar to Fig. 1 except that the smooth crossover between the A_+ and A_- phases along the dotted line is now replaced by a second order transition. This fact can be verified easily, for example, in the case of $\tilde{B} = 0$ by setting $n_+ = n_- = 1/2$ in (3.2) and (3.3) and rewriting these equations for the combination $m_+^z - m_-^z$.

Finally, we note that the results (3.1), (3.2) and (3.3) are valid not only in the limit $\Delta \to \infty$, but for *all* $\Delta > 0$, as long as both sublattice magnetizations m_+ and m_- point along the z-axis. This means that the properties of the A_+ and A_- phases are independent of Δ when expressed as functions of $\tilde{B}$ and $\tilde{T}$. In particular, the first order A_+–A_- transition as well as the first order transition at $\tilde{B} = 0$, $\tilde{T} < 1$ will be present in all phase diagrams unless "masked" by other phases.

3.2 Heisenberg model ($\Delta = 1$)

In the Heisenberg case $\Delta = 1$, the coupling matrix (2.11) is isotropic, and the free energy (2.6) can be rewritten as

$$f = -Tn_+ s(m_+) - Tn_- s(m_-) + \frac{1}{2}m^2$$
$$- n_+^2 m_+^2 - n_-^2 m_-^2 - Bm_z, \quad (3.5)$$

where $m_\pm = |\mathrm{m}_\pm|$, and m and m_z denote the modulus and z-component, respectively, of the average magnetization

$$\mathrm{m} = n_+ \mathrm{m}_+ + n_- \mathrm{m}_-$$

of all spins. The only dependence on the orientation of the magnetizations is through the last term, which takes its minimal value $-Bm$ (remember that we assume $B \geq 0$) when $m_z = m$, i.e., when m is parallel to B. This gives the free energy

$$f = -Tn_+ s(m_+) - Tn_- s(m_-) + \frac{1}{2}m^2$$
$$- n_+^2 m_+^2 - n_-^2 m_-^2 - Bm \quad (3.6)$$

which needs to be minimized subject to the constraints $|n_+ m_+ - n_- m_-| \leq m \leq n_+ m_+ + n_- m_-$. Note that the values of m_+, m_- and m determine the orientations of the magnetizations uniquely. This is clear geometrically because $n_+ \mathrm{m}_+$, $n_- \mathrm{m}_-$ and m all lie in the same plane (the xz-plane, by our assumption that $m_+^y = m_-^y = 0$) and form a rigid parallelogram; see Fig. 2. The angle of a possible rotation of this parallelogram about the origin is fixed by the requirement that m must be parallel to B (i.e., along the positive z-axis for $B > 0$). The remaining indeterminacy with respect to a reflection about the z-axis is removed by our assumption that $m_+^x \geq 0$.

Focussing now on the minimization of (3.6) with respect to m, we note that for $B > n_- m_+ + n_- m_-$ this minimum occurs at the maximum value of m, $m = n_+ m_+ + n_- m_-$. Geometrically, this implies that both m_+ and m_- are directed along the positive z-axis, so we have an A_+ phase. The free energy becomes

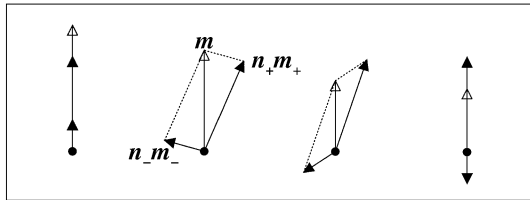$$f = -Tn_+ s(m_+) - Tn_- s(m_-) - \frac{1}{2}(n_+ m_+ - n_- m_-)^2$$
$$- B(n_+ m_+ + n_- m_-),$$

Fig. 2. Geometry of the magnetizations for the Heisenberg model. Shown are (in the xy-plane) the total magnetization $\mathrm{m} = n_+\mathrm{m}_+ + n_-\mathrm{m}_-$ and the sublattice magnetizations scaled by the fractions of spins in the two sublattices, $n_+\mathrm{m}_+$ and $n_-\mathrm{m}_-$. The moduli of the sublattice magnetizations $m_+ = |\mathrm{m}_+|$ and $m_- = |\mathrm{m}_-|$ are kept constant while $m = |\mathrm{m}|$ is decreased from left to right. For the maximum value of m, we have an A_+ phase (left), then we obtain an R phase, with m_- rotating from the positive (upward) towards the negative (downward) z-axis. Finally, when m assumes its minimal value (right), we obtain an A_- phase. This kind of sequence is observed when passing through the R phase in the Heisenberg phase diagram by decreasing the field B at constant T; the moduli of the sublattice magnetizations remain constant, and they rotate in such a way as to keep m pointing along the direction of the field (the z-direction).

and the sublattice magnetizations therefore obey

$$m_+ = \tanh[(n_+m_+ - n_-m_- + B)/T], \qquad (3.7)$$

$$m_- = \tanh[(-n_+m_+ + n_-m_- + B)/T]. \qquad (3.8)$$

For small fields obeying $B < n_+m_+ - n_-m_-$, on the other hand, f is minimized at the minimum value of m, $m = n_+m_+ - n_-m_-$. With m_- now pointing along the negative z-axis, we have an A_- phase with free energy

$$f = -Tn_+s(m_+) - Tn_-s(m_-) - \frac{1}{2}(n_+m_+ + n_-m_-)^2$$
$$-B(n_+m_+ - n_-m_-),$$

and corresponding self-consistency equations

$$m_+ = \tanh[(n_+m_+ + n_-m_- + B)/T], \qquad (3.9)$$

$$m_- = \tanh[(n_+m_+ + n_-m_- - B)/T]. \qquad (3.10)$$

The above results are identical to (3.1), (3.2) and (3.3) for the Ising case, bearing in mind that $\Delta = 1$ and $m_+ = m_+^z$ here, and that $m_-^z = \pm m_-$ in the A_+ and A_- phases, respectively. This conclusion agrees with our general statement in §3.1 that properties of the A_+ and A_- phases are independent of Δ.

For intermediate values of B, finally, the minimum of the free energy (3.6) occurs at a non-extremal value of m. In this regime, we have a new, *rotated* (R) phase where neither m_+ nor m_- point along the z-axis. Minimization of (3.6) with respect to m gives now $m = B$, and thus

$$f = -Tn_+s(m_+) - Tn_-s(m_-)$$
$$-n_+^2 m_+^2 - n_-^2 m_-^2 - \frac{1}{2}B^2.$$

Stationarity with respect to m_+ and m_- yields the self-consistency conditions

$$m_+ = \tanh(2n_+m_+/T)$$
$$m_- = \tanh(2n_-m_-/T) \qquad (3.11)$$

in which the moduli of the sublattice magnetizations are decoupled and the field B no longer appears. This may seem surprising at first, but has a simple explanation: From (2.9) and (2.10), the effective fields that determine the sublattice magnetizations are (using $\mathrm{J} = \mathbf{1}$ for $\Delta = 1$)

$$\mathrm{h}_\pm = \pm(n_+\mathrm{m}_+ - n_-\mathrm{m}_-) + \mathrm{B}.$$

But in the R phase, $\mathrm{m} = \mathrm{B}$, so that

$$\mathrm{h}_\pm = \pm(n_+\mathrm{m}_+ - n_-\mathrm{m}_-) + (n_+\mathrm{m}_+ + n_-\mathrm{m}_-)$$
$$= 2n_\pm\mathrm{m}_\pm,$$

and the coupling of the sublattices and dependence on B disappear, in agreement with (3.11). The geometrical implication of (3.11) is that only the orientations but not the moduli of the sublattice magnetizations change as the R phase is traversed. Figure 2 shows that as m (and thus B) decreases, m_- rotates away from the positive z-axis and towards the negative z-axis; when it reaches the latter, a transition to an A_- phase occurs. The magnetization of the positive sublattice, m_+, first rotates away from the z-axis and then back towards it; this follows from the fact that $\mathrm{m} = n_+m_+ + n_-m_-$ must keep pointing along the positive z-axis.

Above, the A_+–R and R–A_- phase boundaries were given as $B = n_+m_+ \pm n_-m_-$, respectively. At $T = 0$, where $m_+ = m_- = 1$, these reduce to $B = n_+ + n_- = 1$ and $B = n_+ - n_- = \epsilon$; for nonzero temperatures, we have to find the phase boundaries numerically by solving the relevant self-consistency equations for m_+ and m_-. We then find (see Fig. 3) that there is a line of second order transitions connecting the zero-temperature A_+–R and R–A_- transitions; the R phase only occurs inside the "loop" formed by this line. The only other feature of the phase diagram is the first-order transition line at $B = 0$, $T < 1$, which is identical to the one found for the Ising case.

3.3 XY model ($\Delta = 0$)

As the final "simple" case we consider the XY version of our model, which is obtained for $\Delta = 0$. In this case it is convenient to introduce the mirror image (in the xy-plane) of m_- about the z-axis, given by $\vec{\mathrm{m}}_- = (-m_-^x, 0, m_-^z)$, and the corresponding total (pseudo-) magnetization $\vec{\mathrm{m}} = n_+\mathrm{m}_+ + n_-\vec{\mathrm{m}}_-$. In these variables, the free energy (2.6) becomes

$$f = -Tn_+s(m_+) - Tn_-s(\tilde{m}_-) - \frac{1}{2}\tilde{m}_x^2 - B\tilde{m}_z$$
$$= -Tn_+s(m_+) - Tn_-s(\tilde{m}_-)$$
$$-\frac{1}{2}\tilde{m}^2 + \frac{1}{2}\tilde{m}_z^2 - B\tilde{m}_z. \qquad (3.12)$$

Minimizing over the allowed values of $\tilde{m}_z \in [-\tilde{m}, \tilde{m}]$ gives $\tilde{m}_z = B$ as long as $B \leq \tilde{m}$. The last two terms in (3.12) then reduce to the constant $-B^2/2$, and the remainder of the free energy is minimized (for
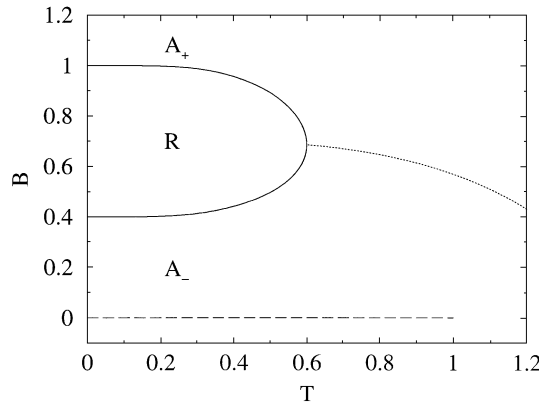
Fig. 3. Phase diagram for the Heisenberg case $\Delta = 1$, for $\epsilon = 0.4$. The dashed line shows the conventional first order transition at $B = 0$, where all magnetizations change sign; the solid line is a line of second order transitions between aligned (A_+ or A_-) and rotated (R) phases. The sublattice magnetization m_- passes smoothly through zero on the dotted line.

Fig. 4. Phase diagram for the XY case $\Delta = 0$. The solid line indicates the second order transition between the rotated (R) and the aligned (A_+) phases. Note that this phase diagram is independent of ϵ, i.e., of the amount of disorder.

given m_+ and $\tilde{m}_-$) when $\tilde{m}$ takes its maximum value $\tilde{m} = n_+ m_+ + n_- \tilde{m}_-$. Geometrically, this means that m_+, $\vec{\mathrm{m}}_-$ and $\vec{\mathrm{m}}$ are all parallel to each other. The free energy is

$$ f = -T n_+ s(m_+) - T n_- s(\tilde{m}_-) $$
$$ - \frac{1}{2}(n_+ m_+ + n_- \tilde{m}_-)^2 - \frac{1}{2}B^2, $$

while the stationarity conditions

$$ m_+ = \tanh[(n_+ m_+ + n_- \tilde{m}_-)/T] $$
$$ \tilde{m}_- = \tanh[(n_+ m_+ + n_- \tilde{m}_-)/T] $$

show that $m_+ = \tilde{m}_-$, hence also $\tilde{m} = m_+ = \tilde{m}_-$ with $\tilde{m} = \tanh(\tilde{m}/T)$. The three vectors m_+, $\vec{\mathrm{m}}_-$ and $\vec{\mathrm{m}}_-$ are therefore not just parallel, but in fact identical; their orientation in the xz-plane is given by the ratio of $\tilde{m}_z = B$ and $\tilde{m}$. Reverting to the original vectors, we have that m_+ and m_- are rotated away from the z-axis and are mirror images of each other under a reflection about this axis; we therefore have an R phase. The average magnetization m always points along the positive z-axis. Starting from $B = 0$, m_- and m_+ are directed along the negative and positive x-axes, respectively (this follows from $\tilde{m}^z = 0$ and $m_+^x \geq 0$). As B is increased, both sublattice magnetizations rotate towards the z-axis which they reach at the point where $B = \tilde{m}$.

For larger B, we have an A_+ phase. In this phase, $\tilde{m}_z = \tilde{m}$; inserting this into (3.12), the minimum with respect to $\tilde{m}$ is again reached for $\tilde{m} = n_+ m_+ + n_- \tilde{m}_-$, giving

$$ f = -T n_+ s(m_+) - T n_- s(\tilde{m}_-) - B(n_+ m_+ + n_- \tilde{m}_-), $$

and thus $m_+ = \tilde{m}_- = \tilde{m} = \tanh(B/T)$. All vectors m_+, $\vec{\mathrm{m}}_-$ and $\vec{\mathrm{m}}_-$ are again identical to each other; because they are now oriented along the z-axis, the same is true of the original magnetizations m_+, m_- and m. In Fig. 4, we show the resulting phase diagram; as expected, there is a line of second order transitions between the R and A_+ phases. Note that obtaining this line numerically is
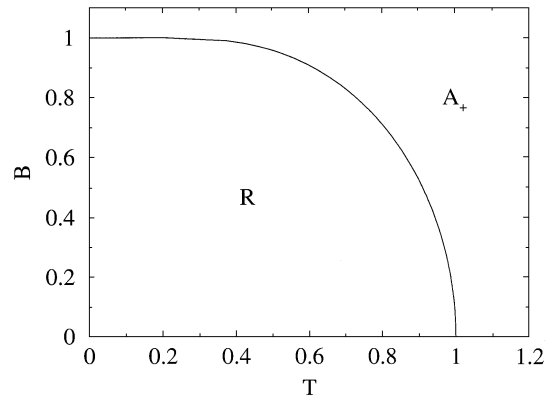
trivial for the XY model: Combining $\tilde{m} = \tanh(\tilde{m}/T)$ and $B = \tilde{m}$ gives $B = \tanh(B/T)$. It follows in particular that in the XY limit, the phase diagram is actually independent of the amount of disorder (as specified by ϵ).

It may appear strange that the disorder has no effect on phase behaviour in the XY limit $\Delta = 0$. But there is in fact again a very simple explanation for this. In the model (2.1), make a gauge transformation *only on the x and y-components* of the spins, $\sigma_i^x \to \xi_i \sigma_i^x$, $\sigma_i^y \to \xi_i \sigma_i^y$. This leaves the commutation relations (2.2) unaffected; indeed, it is just a rotation by π around the z-axis of the spins with $\xi = -1$. But this transformation actually gauges away the disorder completely, so all results must be independent of ϵ, in agreement with our findings above. Note that this argument relies on the fact that only the x- and y-components of the spins appear in the disordered (interaction) part of the Hamiltonian (2.1), and is therefore restricted to $\Delta = 0$.

§4.   Phase Behaviour for General Ͻ

We now turn to the study of our model (2.1) for general values of Δ. The differences in the phase diagrams for the three cases studied above ($\Delta = 0$, 1 and ∞) already suggest that nontrivial phase behaviour may occur for intermediate values of Δ. To orient ourselves, we consider first the zero temperature limit, using Δ and B as the axes of our phase diagram (and considering ϵ as fixed).

For large Δ, we expect essentially Ising behaviour, with an A_+ phase for large B, a first order transition to A_- at $B = n_+ \Delta$, and the conventional first order transition at $B = 0$ where all magnetizations change sign. In fact, as explained in §3.1, this will be the zero temperature phase behaviour for general Δ unless other phases intervene. We therefore study next the limits of stability (i.e., the spinodals) of the A_+ and A_- phases with respect to a transition to the R phase. This is easiest if we write the sublattice magnetizations as

$$\mathrm{m}_+ = m_+(\sin\phi_+, 0, \cos\phi_+) \qquad (4.1)$$

$$\mathrm{m}_- = m_-(-\sin\phi_-, 0, \cos\phi_-). \qquad (4.2)$$

Here $\phi_\pm$ are the angles (in the xz-plane) that m_+ and m_- make with the z-axis; the signs of the angles were chosen such that our conventions $m_+^x \geq 0$ and $m_-^x \leq 0$ always imply non-negative angles. Using that $m_+ = m_- = 1$ at $T = 0$, the free energy (2.6) thus simplifies to

$$f = -\frac{1}{2}(n_+ \sin\phi_+ + n_- \sin\phi_-)^2$$
$$-\frac{1}{2}\Delta(n_+ \cos\phi_+ - n_- \cos\phi_-)^2$$
$$-B(n_+ \cos\phi_+ + n_- \cos\phi_-). \qquad (4.3)$$

With only two order parameters (ϕ_+ and ϕ_-) remaining, it is straightforward to find the matrix of second derivatives of f. The criterion (D·2) implies that a spinodal instability occurs when the determinant of this matrix vanishes. Evaluating the latter for $\phi_+ = \phi_- = 0$, one finds for the spinodal of the A_+ phase the condition

$$B^2 - B + \epsilon^2(\Delta - \Delta^2) = 0, \qquad (4.4)$$

while for the A_- phase ($\phi_+ = 0$, $\phi_- = \pi$) the corresponding result is

$$-B^2 + B\epsilon + \Delta^2 - \Delta = 0. \qquad (4.5)$$

The signs of the expressions on the l.h.s. have been chosen such that they are positive when the phases are stable. Also, because of the symmetry of the free energy (4.3) under $\phi_+ \to -\phi_+$ and $\phi_- \to -\phi_-$ or $\phi_- \to 2\pi - \phi_-$, these spinodals automatically satisfy the critical point criterion (D·5) and so are in fact critical points. Figure 5 shows a plot of the spinodals lines (4.4) and (4.5) for $\epsilon = 0.4$. We see that the A_+ phase is stable for large fields, but destabilizes as B is lowered; the A_- phase, on the other hand, tends to be stable for smaller values of B, and large Δ. Nontrivially, however, the A_- spinodal shows *re-entrance*: For $\Delta \in [\Delta_{\mathrm{re}}, 1]$, with

$$\Delta_{\mathrm{re}} = \frac{1}{2}(1 + \sqrt{1 - \epsilon^2}),$$

eq. (4.5) has two physical solutions for B, so the A_- phase is unstable at zero field, becomes stable at intermediate values of B, and destabilizes again as B is increased further.

In Fig. 5, the first order A_+–A_- transition line $B = n_+\Delta$ is also shown. Moving along this transition line from large to small Δ, the first spinodal which one crosses is that of the A_+ phase, at the value of Δ given by

$$\Delta_{\mathrm{Ising}} = 2\frac{2\epsilon + 1}{3\epsilon + 1}.$$

For large values of Δ, the instabilities of the A_+ and A_- phases are therefore pre-empted by the first order A_+–A_- transition. In this regime, we expect pure Ising behaviour even at non-zero temperature, and this is indeed what we find (see below).

Now consider a value of Δ just below Δ_{Ising}. The A_- phase is stable for $B = 0$, and remains so until at $B = n_+\Delta$ the free energy of the A_+ phase becomes
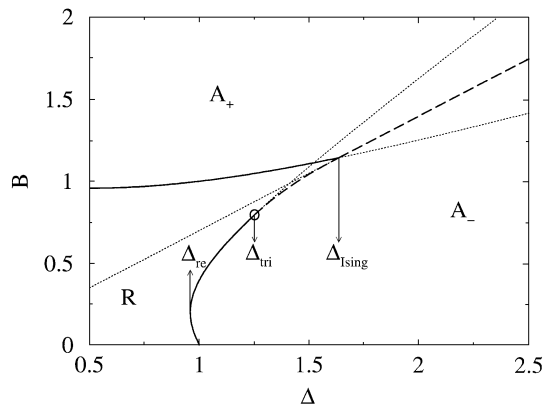

Fig. 5. Zero temperature phase diagram for $\epsilon = 0.4$. The transitions between the three phases A_+, A_- and R are indicated by bold lines (solid for second order, dashed for first order). Dotted lines show the continuations of the phase boundaries into metastable or unstable regimes. Note that the A_-–R transition is re-entrant for $\Delta_{\mathrm{re}} < \Delta < 1$. Also, for $\Delta_{\mathrm{tri}} < \Delta < \Delta_{\mathrm{Ising}}$, the first order A_+–A_- transition is—because of the instability of the A_+ phase—pre-empted by a first order transition from A_- to R. Below Δ_{tri}, this transition is second order, implying that at $\Delta = \Delta_{\mathrm{tri}}$ there is a tricritical point (marked by the circle).

lower. The latter is still unstable, however, because we are below the A_+ spinodal. There must therefore be a stable phase with lower free energy. This phase can only be an R phase (it is neither A_+ nor A_-), and a first order transition to this phase must actually occur at $B < n_+\Delta$. This implies that there is a line of first order A_-–R transitions extending to the left of the point $\Delta = \Delta_{\mathrm{Ising}}, B = n_+\Delta_{\mathrm{Ising}}$. Where this line meets the A_- spinodal (i.e., the line of second order transitions between A_- and R), there will be a *tricritical* point. Applying the criterion (D·6) to the free energy (4.3), one finds after some algebra that this point obeys, in addition to (4.5),

$$B^2 = \Delta(\Delta - 1)(4\Delta - 3).$$

It can be shown that, as ϵ varies between 0 and 1, this tricritical point moves smoothly from $\Delta = 1, B = 0$ to $\Delta = 3/2, B = 3/2$. In particular, if we call Δ_{tri} the value of Δ at the tricritical point, we have $1 < \Delta_{\mathrm{tri}} < 3/2 < \Delta_{\mathrm{Ising}} < 2$ for all ϵ.

Having clarified the structure of the zero temperature phase diagram, we can now move on to the finite temperature case. The numerical results we show were obtained as follows: For spinodals and tricritical points, we derived analytically the form of the relevant conditions (D·2) and (D·6) (for our free energy (2.6) with the four order parameters m_+^z, m_-^z, m_+^x and m_-^x). We then solved these numerically, along with the self-consistency equations (2.9). First order transitions were located as usual by comparing the free energies of the relevant phases. All results were obtained from double-precision routines for solving nonlinear simultaneous equations, and cross-checked using a symbolic manipulation software package with "arbitrary precision" floating point operations. We can distinguish a total of seven different phase diagram topologies, depending on the value of Δ:
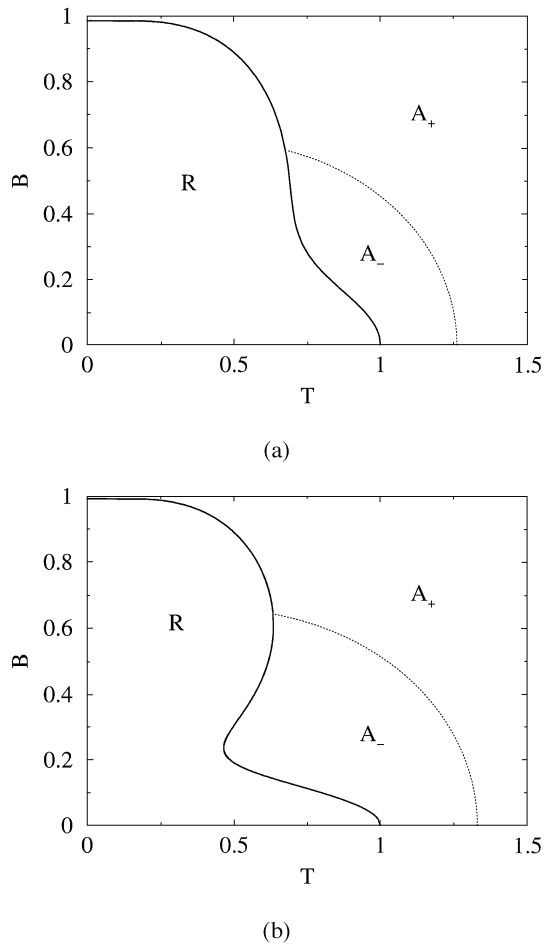
(a)

(b)

Fig. 6. Phase diagrams in regime 1 ($\Delta < \Delta_{\mathrm{re}}$) for $\epsilon = 0.4$. The solid lines mark second order transitions between the phases. As in Fig. 1, the dotted lines show where the A_- and A_+ phases transform smoothly into each other ($m_-^z = 0$). For small Δ (top, $\Delta = 0.9$), the phase diagram resembles qualitatively that of the XY model (Fig. 4). In the bottom graph, $\Delta = 0.95$ is close to $\Delta_{\mathrm{re}} = 0.958\ldots$, and re-entrant behaviour appears at nonzero temperature. This is a precursor of the transition to regime 2.

Regime 1: XY-like behaviour ($0 \le \Delta < \Delta_{\mathrm{re}}$). For small values of Δ, the phase diagram has essentially the same features as for the XY limit $\Delta \to 0$; an example is shown in Fig. 6. It is clear that this behaviour cannot persist up to $\Delta = 1$, however: From the zero temperature phase diagram, we know that for $\Delta_{\mathrm{re}} < \Delta < 1$, there must be re-entrant behaviour. Correspondingly, the second order R–A_+ transition line must develop a "dent"—as if someone was pushing against it from the positive T-direction—as Δ increases; this dent will reach $T = 0$ exactly at $\Delta = \Delta_{\mathrm{re}}$. Before this happens, re-entrance will already be visible for nonzero T; Fig. 6 confirms this. In principle, one could use the appearance of re-entrance at nonzero T to further divide this regime into two sub-regimes, but we choose not to do so because the overall topology of the phase diagram remains unchanged.

To clarify the physical nature of the observed re-entrance, we show in Fig. 7 the B-dependence of the angles $\phi_\pm$ which the sublattice magnetizations m_+ and m_- make with the z-axis. The two sets of curves correspond to vertical cuts through Fig. 6 (bottom), at tem-
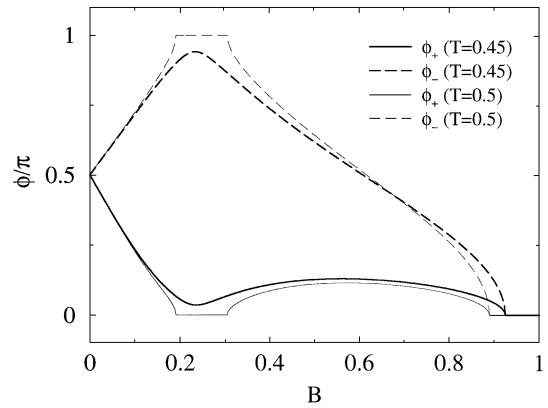

Fig. 7. The dependence of the angles $\phi_\pm$ of the sublattice magnetizations on the field B, at constant temperature T. The parameters $\epsilon = 0.4$, $\Delta = 0.95$ are as in Fig. 6 (bottom). Two sets of curves are shown, for $T = 0.45$ and 0.5; these correspond to vertical cuts through Fig. 6 (bottom) just below and just above the temperature where re-entrance at constant T is first observed.

peratures just below and just above the appearance of the re-entrance. Bearing in mind the definitions (4.1), (4.2) of $\phi_\pm$, we see that m_+ and m_- start off at $B = 0$ by pointing along the positive and negative x-axis, respectively. As B is increased, they both rotate *counter-clockwise* at first. Below the re-entrance, this rotation stops before either of the two magnetizations reaches the z-axis, and reverses. Eventually, both m_+ and m_- then rotate towards the positive z-axis, reaching it at the R–A_+ transition. The behaviour above the re-entrance is now recognized as a more extreme form of this, where the initial counter-clockwise rotation of the two magnetizations continues until m_+ and m_- point along the positive and negative z-directions, respectively. This gives the R–A_- transition; when the reversal of the counter-clockwise motion sets in, both m_+ and m_- eventually 'detach' again from the z-axis, marking the transition back to the R phase. The behaviour as B is increased further then resembles that below the re-entrance, resulting in the final R–A_+ transition.

Regime 2: Between XY and Heisenberg ($\Delta_{\mathrm{re}} < \Delta < 1$). At $\Delta = \Delta_{\mathrm{re}}$, the R–$A_+$ transition line "pinches off" at the B-axis; for larger Δ, we therefore have two separate transition lines of this kind (see Fig. 8). For low enough temperatures, the sequence of phases observed as B is increased from 0 is therefore R–A_-–R–A_+. As the Heisenberg case $\Delta = 1$ is approached, the R–A_- transition line (a loop, if we bear in mind its mirror image for negative B) moves closer to the horizontal axis $B = 0$ and at $\Delta = 1$ collapses into the first order transition line of Fig. 3. The latter exists for all $\Delta \ge 1$ (extending up to $\tilde{T} = 1$, i.e., $T = \Delta$, as expected from our discussion of the Ising case) and will not be mentioned explicitly in the following.

Regime 3: Heisenberg-like ($1 \le \Delta < \Delta_{\mathrm{tri}}$). To make the eventual connection with the Ising limit $\Delta \to \infty$ more apparent, we will use the rescaled variables $\tilde{T} = T/\Delta$ and $\tilde{B} = B/\Delta$ as the axes of all phase diagrams from now on. In the numerical examples, we also switch from $\epsilon = 0.4$ to $\epsilon = 0.01$, where the intermediate regimes
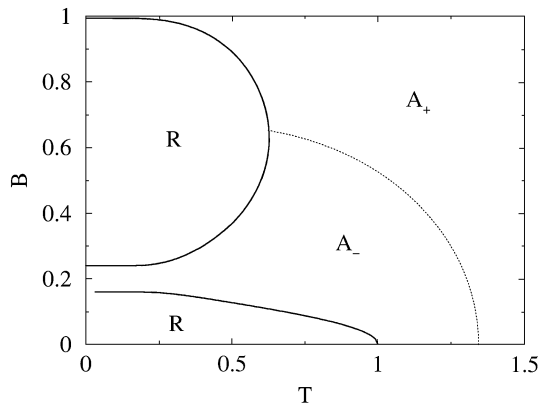
Fig. 8. Phase diagram in regime 2 ($\Delta_{\mathrm{re}} < \Delta < 1$), for $\epsilon = 0.4$ (where $\Delta_{\mathrm{re}} = 0.958\ldots$) and $\Delta = 0.96$. The lines have the same meaning as in Fig. 6. Re-entrant behaviour now occurs even at zero temperature.
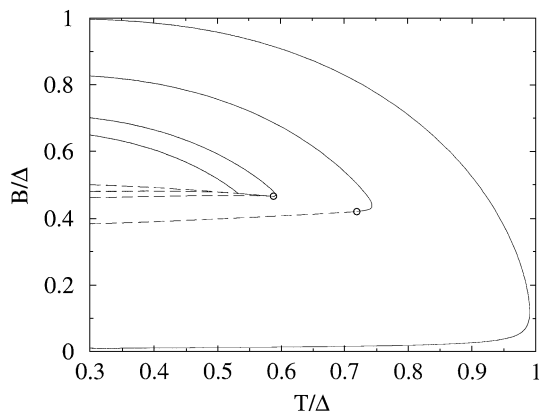

Fig. 10. Detail of a phase diagram in regime 5 ($\Delta = 1.4$, $\epsilon = 0.01$). Solid and dashed lines mark second and first order transitions, respectively; circles indicate tricritical points. There is a three-phase point where the three first order lines meet.

Fig. 9. Phase diagrams in regimes 3–7 ($\Delta = 1$, 1.2, 1.4, 1.5, 2 from the outside to the inside), for $\epsilon = 0.01$. Solid and dashed lines mark second and first order transitions, respectively; the circle indicates a tricritical point. See following figures for details.
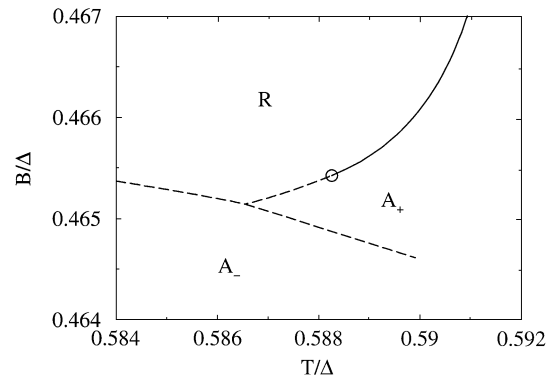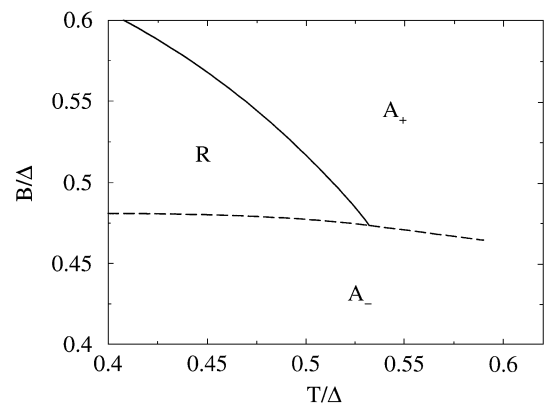

Fig. 11. Detail of a phase diagram in regime 6 ($\Delta = 1.5$, $\epsilon = 0.01$). Solid and dashed lines mark second and first order transitions, respectively. There is a critical end point where the line of second order transitions meets the first order line.

explained below are somewhat easier to visualize. In the regime $1 \le \Delta < \Delta_{\mathrm{tri}}$, the phase diagram has qualitatively the same shape as for the Heisenberg case $\Delta = 1$: A loop of second order transitions between R and A_+ or A_-, respectively, beginning and ending on the $\tilde{B}$-axis (see Fig. 9). At $\Delta = \Delta_{\mathrm{tri}}$, the tricritical point that we found earlier appears on the $\tilde{T} = 0$ axis, marking the transition to the next regime.

Regime 4: Tricritical ($\Delta_{\mathrm{tri}} < \Delta < \Delta_3$). As Δ increases, the tricritical point moves out to larger $\tilde{T}$. To the left of it, the A_-–R transition is now first order (see Fig. 9). One might naively expect that as Δ is increased further towards the Ising limit of large Δ, the "loop" of transitions between R and A_- or A_+ would simply collapse at Δ_{Ising} onto the Ising first order A_+–A_- transition line. In fact, two other regimes appear first.

Regime 5: Tricritical plus three-phase ($\Delta_3 < \Delta < \Delta_{\mathrm{CEP}}$). It turns out that the R–A transition loop with the tricritical point on it does not just shrink along the $\tilde{B}$ direction, but also moves towards smaller values of $\tilde{T}$ as Δ is increased. Eventually, at some Δ_3, the Ising A_+–A_-

transition line therefore "pokes" through the loop. This must happen at a point where the transition is first order; at a point with a second order transition this would be impossible, as it would imply a first order transition between two phases which are actually identical, being both in critical coexistence with the same third phase. This means that one has a point where three phase transition lines meet, i.e., a *three-phase point*; see Fig. 10. There is still a tricritical point where the R–A_+ phase transition changes from second to first order. Note that this regime generally corresponds to only a very small range of Δ; for $\epsilon = 0.01$, we estimate $\Delta_3 \approx 1.39$ and $\Delta_{\mathrm{CEP}} \approx 1.41$.

Regime 6: Critical end point ($\Delta_{\mathrm{CEP}} < \Delta < \Delta_{\mathrm{Ising}}$). The relative positions of the tricritical and three-phase points in the previous regime change as Δ increases, until at some Δ_{CEP} they coincide. From there onwards, the tricritical point is no longer accessible (it is in a metastable or unstable part of the phase diagram). Instead, as shown in Fig. 11, one now has a line of second order A_+–R transitions that meets a line of first order transitions (between A_- and R for small $\tilde{T}$, and between A_- and A_+ for large $\tilde{T}$) at a *critical end point*. As Δ
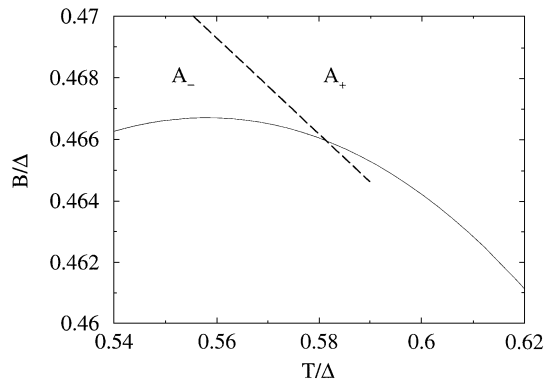
Fig. 12. The transition between regimes 5 and 6, for $\epsilon = 0.01$. The dashed line shows the Ising A_+–A_- transition line (which, when plotted in terms of $\tilde{B} = B/\Delta$ and $\tilde{T} = T/\Delta$ as done here, is independent of Δ). The solid line shows the curve traversed by the tricritical point as Δ is varied, moving from right to left with increasing Δ. The crossing of the two curves (i.e., the value of Δ for which the tricritical point meets the A_+–A_- transition and thus turns into a critical end point) defines Δ_{CEP}. Note that for lower values of Δ than shown here, the tricritical point would first continue to move right, but eventually swing back towards the $\tilde{B}$-axis, meeting the latter at $\Delta = \Delta_{\mathrm{tri}}$.

increases, this point shifts towards lower temperatures and eventually disappears at $\Delta = \Delta_{\mathrm{Ising}}$. Figure 12 illustrates the transition between regimes 5 and 6 by showing the curve traversed by the tricritical point as Δ is varied, together with the Ising A_+–A_- transition line. The value of Δ where these two curves meet (i.e., where the tricritical point "collides" with the A_+–A_- transition and thus turns into a critical end point) defines Δ_{CEP}.

Regime 7: Ising-like ($\Delta \geq \Delta_{\mathrm{Ising}}$). Finally, for large values of Δ, one has pure Ising behaviour, with a Δ-independent phase diagram (when represented in terms of $\tilde{B}$ and $\tilde{T}$) exhibiting the by now familiar line of first order A_+–A_- transitions (see Fig. 1).

§5. Conclusion

We have solved the infinite-range quantum Mattis model by a variational method that gives the exact solution in the thermodynamic limit. The model has various interesting aspects such as randomness (although without frustration), quantum effects and competition between exchange interaction and external field. We found three ordered phases, two of which have spin states collinear with the external field and the remaining one with non-collinear rotated spin states. The phase diagram has a very rich structure depending upon the various parameters, in particular the anisotropy of the interaction.

We now ask how important quantum effects are in producing the intricate macroscopic behaviour of the system. The form of the entropy term in the free energy (2.6) is a direct consequence of the spin-1/2 characteristics of a single quantum spin. The energy term, on the other hand, is of the form one would expect classically. Thus it is clear that the $T = 0$ properties do not reflect quantum effects. Finite-temperature behaviour, on the other hand, could be affected by quantum fluctuations. This fact is somewhat counter-intuitive since

quantum effects are usually most important at *low* rather than high temperatures. An interesting manifestation of finite-temperature quantum effects is seen in the equations of state (3.8) to (3.10) of the Heisenberg model in the A_+ and A_- phases. These equations of state have exactly the same form as for the Ising case (3.2) and (3.3), which would not be the case if the spins in the Heisenberg model were classical vectors. The transverse (i.e. x and y) components of the spin-1/2 operator have disappeared and only the z component comes into play, as would be expected for a single quantum spin in a classical field.

We stress that, even though the quantum nature of the individual spins in the model does manifest itself at finite temperatures, this does not produce any qualitatively new ordered phases beyond those already found at $T = 0$. The possible types of ordering are thus determined by the classical considerations for the ground state; quantum effects only control how these ordered phases and the boundaries between them are arranged in the finite temperature phase diagrams.

Finally, a natural question that arises is how our results would change in the more physically realistic case of finite range interactions (corresponding to finite dimensionality of the system). While we cannot give a definite answer to this question at this point, existing investigations of finite-dimensional quantum Mattis model[4, 5] do suggest that the classical picture gives reasonable predictions for some features of the model. On the basis of these results, we conjecture that our observations for the infinite-range model should give an at least qualitatively reliable guide to the finite-dimensional problem. Future work is obviously needed to clarify this point.

Appendix A: Self-Consistency of Mean Field Approximation

In this appendix, we show that mean field theory gives exact results for the generalized Mattis model (2.1). The intuitive reason for this is clear: The field that each spin experiences is an average of $O(N)$ other spins and therefore becomes nonfluctuating (and classical) in the thermodynamic limit.

To see more explicitly why the mean field approximation, which assumes that all spins are uncorrelated with each other, becomes self-consistent for $N \to \infty$, we consider a generalization of our original Hamiltonian (2.1) to site-dependent fields:

$$H = -\frac{1}{N} \sum_{i<j} \xi_i \xi_j \sigma_i \cdot \mathbf{J} \, \sigma_j - \sum_i \mathbf{B}_i \cdot \sigma_i.$$

The fluctuation-dissipation theorem then relates the susceptibility matrix to the spin-spin correlations according to

$$\frac{\partial \langle \sigma_i \rangle}{\partial B_j} = -\frac{\partial F}{\partial B_i \partial B_j}$$

$$= \beta \langle \Delta\sigma_i \Delta\sigma_j \rangle, \quad \Delta\sigma_i = \sigma_i - \langle \sigma_i \rangle. \quad (A\cdot1)$$

For given i and j, this is an equality between 3×3 tensors, whose components are written explicitly as $\partial \langle \sigma_i^\alpha \rangle /\partial B_j^\gamma = \beta \langle \Delta\sigma_i^\alpha \Delta\sigma_j^\gamma \rangle$. We can thus verify that mean field theory is self-consistent by working out the susceptibility matrix and using it to show that correlations between different spins vanish for $N \to \infty$.

To obtain the susceptibility matrix, we start from the mean field equations. By a direct generalization of (2.5), these are

$$h_i = B_i + \xi_i J (n_+ m_+ - n_- m_-) - \frac{1}{N} J m_i. \quad (A\cdot2)$$

For the case of site-independent fields $B_i = B$, they reduce to (2.5), with the fields h_i and magnetizations m_i being the same for all spins in each of the two sublattices $I_\pm$ (in the thermodynamic limit). We now add a small perturbation δB to the field of one of the spins; without loss of generality, this spin can be taken as σ_1. For definiteness, we also assume that σ_1 is in the positive sublattice I_+; the calculation for the opposite case is completely analogous. The solution to the mean field equations (A·2) will then be such that all spins in the sublattice I_- still have the same fields h_- and magnetizations m_-. In I_+, on the other hand, we have to distinguish between the field and magnetization of the chosen spin (h_1 and m_1) and those of all other spins in the sublattice; we denote the latter by h_2 and m_2. Using that the average magnetization of this sublattice is now

$$m_+ = \frac{1}{Nn_+}[m_1 + (Nn_+ - 1)m_2]$$

$$= \frac{1}{Nn_+}m_1 + \left(1 - \frac{1}{Nn_+}\right) m_2,$$

the mean field equations (A·2) then take the form

$$h_1 = B + \delta B + J \left[\frac{1}{N}m_1 + \left(n_+ - \frac{1}{N}\right) m_2\right]$$

$$-J n_- m_- - \frac{1}{N} J m_1$$

$$h_2 = B + J \left[\frac{1}{N}m_1 + \left(n_+ - \frac{1}{N}\right) m_2\right]$$

$$-J n_- m_- - \frac{1}{N} J m_2$$

$$h_- = B - J \left[\frac{1}{N}m_1 + \left(n_+ - \frac{1}{N}\right) m_2\right]$$

$$+J \left(n_- - \frac{1}{N}\right) m_-.$$

Subtracting the corresponding equations for $\delta B = 0$ gives relations between the deviations of the fields (δh_1 etc.) and magnetizations (δm_1 etc.) from their values for site-independent fields:

$$\delta h_1 = \delta B + \left(n_+ - \frac{1}{N}\right) J \delta m_2 - n_- J \delta m_-$$

$$\delta h_2 = \frac{1}{N}J \delta m_1 + \left(n_+ - \frac{2}{N}\right) J \delta m_2 - n_- J \delta m_-$$

$$\delta h_- = -\frac{1}{N}J \delta m_1 - \left(n_+ - \frac{1}{N}\right) J \delta m_2$$

$$+ \left(n_- - \frac{1}{N}\right) J \delta m_-.$$

For small δB, we can linearize these using

$$\delta m_1 = \chi_+ \delta h_1, \qquad \delta m_2 = \chi_+ \delta h_2, \qquad \delta m_- = \chi_- \delta h_-,$$

where χ_+ and χ_- are the local susceptibility tensors (2.4) of spins in the two sublattices; because these are evaluated for the unperturbed solution (with site-independent fields B), there is no need to distinguish between χ_1 and χ_2. We thus obtain

$$\chi_+^{-1}\delta m_1 - \left(n_+ - \frac{1}{N}\right) J \delta m_2 + n_- J \delta m_- = \delta B$$

$$-\frac{1}{N}J \delta m_1 + \left[\chi_+^{-1} - \left(n_+ - \frac{2}{N}\right) J\right] \delta m_2 + n_- J \delta m_- = 0$$

$$\frac{1}{N}J \delta m_1 + \left(n_+ - \frac{1}{N}\right) J \delta m_2 + \left[\chi_-^{-1} - \left(n_- - \frac{1}{N}\right) J\right] \delta m_- = 0.$$

These equations can solved explicitly for the changes in the magnetizations; keeping only the leading order terms for $N \to \infty$, one finds

$$\delta m_1 = \chi_+ \delta B$$

$$\delta m_2 = \frac{1}{N}\chi_+ J \left[\mathbf{1} - n_+ \chi_+ J - n_- \chi_- J\right]^{-1} \chi_+ \delta B$$

$$\delta m_- = -\frac{1}{N}\chi_- J \left[\mathbf{1} - n_+ \chi_+ J - n_- \chi_- J\right]^{-1} \chi_+ \delta B.$$

The 3×3 tensors multiplying δB on the r.h.s. give the entries of the susceptibility matrix $\partial m_i/\partial B_j$ (for the case $j = 1 \in I_+$ considered here; as stated above, the case $j \in I_-$ can be treated in exactly the same fashion). We read off that these entries are of $O(1)$ only for $i = j$, while all off-diagonal terms are $O(1/N)$. The fluctuation-dissipation theorem (A·1) then implies that all correlations $\langle \Delta\sigma_i \Delta\sigma_j \rangle$ between different spins $i \neq j$ are $O(1/N)$; in the thermodynamic limit, mean field theory therefore becomes exact.

Appendix B: Direct Solution for a Special Case

It is possible in some cases to derive the variational free energy (2.6) directly from the Hamiltonian (2.1). We consider the example of the Heisenberg model ($\Delta = 1$) here to confirm the variational calculations.

Setting $\hbar = 1$, the Hamiltonian (2.1) can be written in terms of total spin operators as

$$H = -\frac{4}{N}\left(S_+^2 + S_-^2 - \frac{1}{2}S^2\right) - 2BS_z,$$

where we have ignored a trivial constant term. The spin operators are defined by

$$S_\pm = \frac{1}{2}\sum_{i \in I_\pm} \frac{3}{4}_i, \quad S = S_+ + S_-.$$

Because the quartet $\{S_+^2, S_-^2, S^2, S_z\}$ form a set of mutually commuting operators, the Hilbert space of the N-particle system is spanned by their simultaneous eigenspaces $|s_+, s_-; s, m\rangle$. The free energy per spin f_N is therefore

$$f_N = -\frac{T}{N}\ln \sum_{s_+, s_-} d_{N_+}^{s_+} d_{N_-}^{s_-} e^{\frac{4\beta}{N}[s_+(s_++1)+s_-(s_-+1)]}$$

$$\times \sum_{s=|s_+-s_-|}^{s_++s_-} e^{-\frac{2\beta}{N}s(s+1)} \sum_{m=-s}^{s} e^{2m\beta B} \qquad \text{(B·1)}$$

Here the sums over $s_\pm$ run from 0 (or 1/2 if $N_\pm$ is odd) to $N_\pm/2$ ($= n_\pm N/2$). The symbol d_M^n denotes the number of multiplets of total spin n in a system of M spin-$\frac{1}{2}$ particles. We show in Appendix C that d_M^n is given explicitly by

$$d_M^n = \binom{M-1}{\frac{1}{2}M+n-1} - \binom{M-1}{\frac{1}{2}M+n+1}$$

$$= \frac{(2n+1)M!}{(\frac{1}{2}M-n)!(\frac{1}{2}M+n+1)!}. \qquad \text{(B·2)}$$

To evaluate the free energy (B·1), we first carry out the sum over m,

$$\sum_{m=-s}^{s} e^{2m\beta B} = \frac{e^{(2s+1)\beta B} - e^{-(2s+1)\beta B}}{e^{\beta B} - e^{-\beta B}}.$$

Setting $L = \pm\beta B$, we therefore need to evaluate the following sum over s:

$$\sum_{s=|s_+-s_-|}^{s_++s_-} e^{-\frac{2\beta}{N}s(s+1)+(2s+1)L}$$

$$= e^L \int \frac{dz}{\sqrt{2\pi}}\, e^{-\frac{1}{2}z^2} \sum_{s=|s_+-s_-|}^{s_++s_-} e^{2s(L-\beta/N-iz\sqrt{\beta/N})}$$

$$= e^L \int \frac{dz}{\sqrt{2\pi}}\, e^{-\frac{1}{2}z^2} \times \left[\frac{e^{2|s_+-s_-|(L-\beta/N-iz\sqrt{\beta/N})} - e^{2(s_++s_-+1)(L-\beta/N-iz\sqrt{\beta/N})}}{1 - e^{2(L-\beta/N-iz\sqrt{\beta/N})}}\right]$$

Rescaling the integration variable by $\sqrt{\beta N}$, we thus have

$$\sum_{s=|s_+-s_-|}^{s_++s_-} e^{-\frac{2\beta}{N}s(s+1)}\left[e^{(2s+1)\beta B} - e^{-(2s+1)\beta B}\right]$$

$$= \left(\frac{\beta N}{2\pi}\right)^{\frac{1}{2}} \int dz\, e^{-\frac{1}{2}\beta N z^2} \left\{\frac{e^{2\beta|s_+-s_-|(B-1/N-iz)} - e^{2\beta(s_++s_-+1)(B-1/N-iz)}}{e^{-\beta B} - e^{\beta(B-2/N-2iz)}}\right.$$

$$\left. - \frac{e^{2\beta|s_+-s_-|(-B-1/N-iz)} - e^{2\beta(s_++s_-+1)(-B-1/N-iz)}}{e^{\beta B} - e^{\beta(-B-2/N-2iz)}}\right\}.$$

The thermodynamic limit of the free energy is then expressed as

$$f = -\lim_{N\to\infty} \frac{T}{N}\ln \int dz\, e^{-\frac{1}{2}\beta N z^2}$$

$$\times \sum_{s_+, s_-} d_{N_+}^{s_+} d_{N_-}^{s_-} e^{\frac{4\beta}{N}[s_+(s_++1)+s_-(s_-+1)]}$$

$$\times \left\{\frac{e^{2\beta|s_+-s_-|(B-iz)} - e^{2\beta(s_++s_-+1)(B-iz)}}{e^{-\beta B} - e^{\beta(B-2iz)}}\right.$$

$$\left. - \frac{e^{2\beta|s_+-s_-|(-B-iz)} - e^{2\beta(s_++s_-+1)(-B-iz)}}{e^{\beta B} - e^{\beta(-B-2iz)}}\right\}.$$

The sum over $s_\pm$ can be replaced by an integral in the thermodynamic limit:

$$s_\pm = \frac{1}{2}n_\pm m_\pm N, \quad \sum_{s_\pm} \to \frac{1}{2}n_\pm N \int_0^1 dm_\pm.$$

Also, for large N the expression (B·2) for the combinatorial terms d_N^n can be simplified to

$$\frac{1}{N}\ln d_{N_\pm}^{s_\pm} = \frac{1}{N}\ln\left\{\frac{N_\pm!}{[N_\pm(\frac{1}{2}-m_\pm)]![N_\pm(\frac{1}{2}+m_\pm)]!}\right.$$

$$\left. \times \frac{2N_\pm m_\pm + 1}{N_\pm(\frac{1}{2}+m_\pm)+1}\right\}$$

$$= n_\pm s(m_\pm) + O(1/N).$$

The free energy thus becomes

$$f = -\lim_{N \to \infty} \frac{T}{N} \ln \int_{-\infty}^{\infty} \mathrm{d}z \int_0^1 \mathrm{d}m_+ \int_0^1 \mathrm{d}m_- \ \mathrm{e}^{-\beta N f(z, m_+, m_-)}$$

with

$$f(z, m_+, m_-) = \frac{1}{2}z^2 - n_+^2 m_+^2 - n_-^2 m_-^2 - Tn_+ s(m_+) - Tn_- s(m_-)$$

$$- \lim_{N \to \infty} \frac{T}{N} \ln \left\{ \frac{\mathrm{e}^{\beta N |n_+ m_+ - n_- m_-|(-\mathrm{i}z + B)}}{\sinh[\beta(\mathrm{i}z - B)]} - \frac{\mathrm{e}^{\beta N(n_+ m_+ + n_- m_-)(-\mathrm{i}z + B)}}{\sinh[\beta(\mathrm{i}z - B)]} \right.$$

$$\left. - \frac{\mathrm{e}^{\beta N |n_+ m_+ - n_- m_-|(-\mathrm{i}z - B)}}{\sinh[\beta(\mathrm{i}z + B)]} + \frac{\mathrm{e}^{\beta N(n_+ m_+ + n_- m_-)(-\mathrm{i}z - B)}}{\sinh[\beta(\mathrm{i}z + B)]} \right\}.$$

For $N \to \infty$, the third and fourth terms in the curly brackets become exponentially small compared to the first and second terms, respectively, and can therefore be discarded (remember that we assume $B > 0$). If we also make the change of variable $z \to \mathrm{i}z$ (which implies that the free energy is to be maximized with respect to z), we have

$$f(z, m_+, m_-) = -\frac{1}{2}z^2 - n_+^2 m_+^2 - n_-^2 m_-^2 - Tn_+ s(m_+) - Tn_- s(m_-)$$

$$- \lim_{K \to \infty} \frac{1}{K} \ln \left\{ \frac{\mathrm{e}^{K|n_+ m_+ - n_- m_-|(z + B)}}{\sinh[-\beta(z + B)]} + \frac{\mathrm{e}^{K(n_+ m_+ + n_- m_-)(z + B)}}{\sinh[\beta(z + B)]} \right\}.$$

Because $n_+ m_+ + n_- m_- \geq |n_+ m_+ - n_- m_-|$, the first term inside the curly brackets becomes negligible for $z > -B$; conversely, for $z < -B$, the second term can be discarded. We are then left with

$$f(z, m_+, m_-)$$

$$= -\frac{1}{2}z^2 - n_+^2 m_+^2 - n_-^2 m_-^2$$

$$- Tn_+ s(m_+) - Tn_- s(m_-)$$

$$- (z + B) \times \begin{cases} n_+ m_+ + n_- m_- & (z > -B) \\ |n_+ m_+ - n_- m_-| & (z < -B) \end{cases}.$$

$$\text{(B·3)}$$

Taking the derivative of f with respect to z subsequently gives the equations $z = -(n_+ m_+ + n_- m_-)$ if $z > -B$ and $z = -|n_+ m_+ - n_- m_-|$ if $z < -B$. In addition we have a local maximum at $z = -B$ if the z-derivative of f is negative for $z > -B$ and positive for $z < -B$, which translates into the extra solution $z = -B$ appearing for $|n_+ m_+ - n_- m_-| < B < n_+ m_+ + n_- m_-$. In combination the full picture now becomes:

$$\begin{aligned} B < |n_+ m_+ - n_- m_-| : & \quad z = -|n_+ m_+ - n_- m_-| \\ |n_+ m_+ - n_- m_-| < B < n_+ m_+ + n_- m_- : & \quad z = -B \\ B > n_+ m_+ + n_- m_- : & \quad z = -(n_+ m_+ + n_- m_-) \end{aligned} \qquad \text{(B·4)}$$

Elimination of the variable z using the above result leads us to a reduced free energy minimization problem involving $m_\pm$ only, with

$$\begin{aligned} (a) & \quad \text{Phase A}_- : & \quad B < |n_+ m_+ - n_- m_-| \\ (b) & \quad \text{Phase R} : & \quad |n_+ m_+ - n_- m_-| < B < n_+ m_+ + n_- m_- \\ (c) & \quad \text{Phase A}_+ : & \quad B > n_+ m_+ + n_- m_- \end{aligned} \qquad \text{(B·5)}$$

It is straightforward to verify from eqs. (B·3), (B·4) and (B·5) that the free energy in each phase agrees with that given in §3.2.

Appendix C: Degeneracy Factor d_M^n

We derive here the expression (B·2) for the number of multiplets of total spin n in a system of M spin-$\frac{1}{2}$ particles. In other words, d_M^n is the degeneracy of the state $|n, n_z\rangle$, where n is the total spin quantum number and n_z is any of the allowed values $(-n, -n+1, \ldots, n)$ of the z-component of the total spin.

We proceed by induction over M. For $M = 1$, we have $d_M^n = 1$ for $n = 1/2$ and $d_M^n = 0$ otherwise. Now consider a multiplet of spin n in an M-spin system. When one spin-1/2 particle is added, this multiplet splits into exactly one $n + \frac{1}{2}$ and one $n - \frac{1}{2}$ multiplet. The exception is $n = 0$, where only a single $n = \frac{1}{2}$ multiplet is generated. We therefore have

$$d_{M+1}^n = d_M^{n - \frac{1}{2}} + d_M^{n + \frac{1}{2}} \qquad \text{(C·1)}$$

with the boundary condition

$$d_M^n = 0 \quad (n \leq -\frac{1}{2}). \qquad \text{(C·2)}$$

Now consider an unbiased random walk with sites numbered by the integers $l = 2n + 1$ and discrete time $t = M - 1$. The recursion (C·1) then tells us that

$$2^{-(M-1)}d_M^n = p_t(l), \qquad (\text{C·3})$$

where $p_t(l)$ is the site occupation probability at time t of a random walk starting from initial position $l_0 = 2$ at $t = 0$. The boundary condition (C·2) simply corresponds to an absorbing wall at $l = 0$. Without this absorbing wall, one would have

$$p_t(l) = 2^{-t}\begin{pmatrix} t \\ \frac{1}{2}(l - l_0 + t) \end{pmatrix};$$

in the presence of the wall, one simply subtracts the reflected solution in the usual way to get

$$p_t(l) = 2^{-t}\left[\begin{pmatrix} t \\ \frac{1}{2}(l - l_0 + t) \end{pmatrix} - \begin{pmatrix} t \\ \frac{1}{2}(l + l_0 + t) \end{pmatrix}\right].$$

Inserting this into (C·3) immediately gives the desired result (B·2). In writing the above formulae, we use the convention that the binomial coefficient $\binom{n}{k}$ is zero whenever k is non-integer or outside the range $0 \ldots n$.

Appendix D: Criteria for Spinodals, Critical and Tricritical Points

In this appendix, we set out the general criteria that we use to find spinodals, critical points and tricritical points. Rather than the traditional determinant conditions due to Gibbs,[9] we use a formulation due to Brannock[10] which is more convenient, especially for tricritical points.

Let us assume the free energy per spin is given by $f(\hat\psi)$, where $\hat\psi = (\psi_1 \ldots \psi_n)$ is a vector of n (non-conserved) order parameters. Thermodynamic phases correspond to (local) minima of $f(\hat\psi)$ and therefore obey the stationary condition $\nabla f(\hat\psi) = 0$. At a spinodal point, there is in addition an instability direction $\delta\hat\psi$ along which the free energy has zero curvature, implying that the gradient of f remains zero to first order:

$$(\delta\hat\psi \cdot \nabla)\nabla f(\hat\psi) = 0 \qquad \text{(spinodal)}. \qquad (\text{D·1})$$

The condition for such a $\delta\hat\psi$ to exist is

$$|M| = 0, \qquad M = \nabla\nabla f(\hat\psi). \qquad (\text{D·2})$$

At a critical point, the separation between two neighbouring (in the $\hat\psi$-space) stable phases becomes infinitesimal. These phases are separated by an unstable phase (a saddle point of f). Constructing a curve $\hat\psi(s)$ through these three phases (with $\hat\psi(0) = \hat\psi$, the state we are interested in), we see that (the vector-valued function) $\nabla f(\hat\psi(s))$ vanishes at three infinitesimally separated values of s. At the critical point, located at $s = 0$, these three zeros of $\nabla f(\hat\psi(s))$ coincide, so

$$\nabla f(\hat\psi(s)) = O(s^3).$$

Similarly, at a tricritical point we have three stable phases coming together, with two unstable phases between them, so the corresponding criterion is

$$\nabla f(\hat\psi(s)) = O(s^5).$$

Noting that the spinodal criterion (D·1) can be written

as $\nabla f(\hat\psi(s)) = O(s^2)$ for the curve $\hat\psi(s) = \hat\psi + s\delta\hat\psi$, we can summarize all three criteria as follows: If there exists a curve $\hat\psi(s)$ through the point $\hat\psi$ (with $\hat\psi(0) = \hat\psi$) such that

$$\nabla f(\hat\psi(s)) = O(s^l), \qquad (\text{D·3})$$

then for $l = 2, 3, 5$ respectively $\hat\psi$ is a spinodal, critical and tricritical point.

To evaluate the criterion (D·3) in practice, we write it as

$$\left(\frac{d}{ds}\right)^k \nabla f(\hat\psi(s))\bigg|_{s=0} = 0 \qquad \text{for } k = 1\ldots l-1. \quad (\text{D·4})$$

For the spinodal criterion, this reduces to (D·1) if we identify $\delta\hat\psi$ and $\hat\psi'(0)$. For critical points ($l = 3$) one obtains the additional equation

$$\nabla(\delta\hat\psi \cdot \nabla)^2 f(\hat\psi) + \nabla(\hat\psi''(0)\cdot\nabla)f(\hat\psi) = 0.$$

Taking the scalar product with $\delta\hat\psi$ and using (D·1) eliminates the second term, showing that the criterion for critical points is

$$(\delta\hat\psi \cdot \nabla)^3 f(\hat\psi) = 0 \qquad (\text{D·5})$$

together with (D·1). Following a similar procedure, one finds that tricritical points obey the additional condition

$$(\delta\hat\psi \cdot \nabla)^4 f(\hat\psi) - 3v \cdot M^{-1} v = 0 \qquad (\text{D·6})$$

where

$$v = \nabla(\delta\hat\psi \cdot \nabla)^2 f(\hat\psi).$$

Even though the matrix M has a zero eigenvalue ($M\delta\hat\psi = 0$ from (D·1)), the inverse of M in (D·6) is well defined: From (D·5), we have $\delta\hat\psi \cdot v = 0$, so that v is orthogonal to the corresponding eigenspace. Note that while the first term on the l.h.s. of (D·6) is what one might have expected naively, the second term cannot be neglected: It accounts for the fact that the curve $\hat\psi(s)$ passing through the three (infinitesimally separated) stable phases is generally curved rather than straight.

We finally note that (D·6) is derived from (D·4) for $k = 3$. In principle, the equation for $k = 4$ gives an additional condition that tricritical points must obey. Because of symmetries present in our problem, however, this condition is always satisfied in the cases we consider, and so we do not give its explicit form.

1) R. N. Bhatt: *Spin Glasses and Random Fields*, ed. A. P. Young (World Scientific, Singapore, 1998) p. 225.
2) H. Nishimori and Y. Nonomura: J. Phys. Soc. Jpn. **65** (1996) 3780.
3) D. C. Mattis: Phys. Lett. A **56** (1976) 421.
4) D. Sherrington: J. Phys. C **10** (1977) L7.
5) H. Nishimori: J. Stat. Phys. **26** (1981) 839.
6) T. Nattermann: *Spin Glasses and Random Fields*, ed. A. P. Young (World Scientific, Singapore, 1998) p. 277.
7) N. G. Duffield and R. Kühn: J. Phys. A **22** (1989) 4643.
8) A. Aharony: Phys. Rev. B **18** (1978) 3318.
9) J. W. Gibbs: *The Collected Works of J. Willard Gibbs*; *The Scientific Papers of J. Willard Gibbs*, reprinted (Dover, New York, 1960).
10) G. R. Brannock, J. Chem. Phys. **95** (1991) 612.